arXiv:1204.5257v1 [cond-mat.supr-con] 24 Apr 2012

Little-Parks oscillations near a persistent current loop

Rodolpho Ribeiro Gomes,[1] Isaías G. de Oliveira,[2] and Mauro M. Doria[3]

[1] *Centro Brasileiro de Pesquisas Físicas, 22290-160 Rio de Janeiro RJ Brazil*
[2] *Departamento de Física, Universidade Federal Rural do Rio de Janeiro, 23890-000 Seropédica RJ Brazil*
[3] *Departamento de Física dos Sólidos, Universidade Federal do Rio de Janeiro, 21941-972 Rio de Janeiro RJ, Brazil**

We investigate the Little-Parks oscillations caused by a persistent current loop set on the top edge of a mesoscopic superconducting thin-walled cylinder with a finite height. For a short cylinder the Little-Parks oscillations are approximately the same ones of the standard effect, as there is only one magnetic flux piercing the cylinder. For a tall cylinder the inhomogeneity of the magnetic field makes different magnetic fluxes pierce the cylinder at distinct heights and we show here that this produces two distinct Little-Parks oscillatory regimes according to the persistent current loop. We show that these two regimes, and also the transition between them, are observable in current measurements done in the superconducting cylinder. The two regimes stem from different behavior along the height, as seen in the order parameter, numerically obtained from the Ginzburg-Landau theory through the finite element method.

PACS numbers: 74.78.Na,74.25.-q,74.20.De
Keywords: Ginzburg-Landau theory,mesoscopic superconductor,vortex

I. INTRODUCTION

In the last decades we have witnessed a huge progress in the microfabrication of systems and measurement techniques that have allowed the study of mesoscopic superconducting structures[1]. The critical temperature of a superconducting ring oscillates according to the applied external magnetic field, as shown by Little and Parks (LP) in 1962[2]. The LP effect can be regarded as a forerunner of recent developments[3], because of its eminently mesoscopic nature. It predicts that for a thin-walled cylinder of radius R, the critical temperature varies as $\Delta T_c = (\hbar^2/8mR^2)(\Phi/\Phi_0 - n)^2$, where m is the Copper pair mass, Φ_0 is the fundamental flux, $\Phi = H\,\pi R^2$ is the magnetic flux trapped inside the ring, and n describes a quantum number. A temperature variation detectable within experimental range, say $\Delta Tc \sim 10^{-5}$ K, means that the radius must be in the mesoscopic domain, $R \sim 1.0\mu$m. The LP oscillations are detected by measuring two consecutive temperature maxima, each occurring for $\Delta T_c = 0$, when the total magnetic flux Φ, which is the sum of the external magnetic flux piercing a given surface and the magnetic flux produced by the circulation of the screening supercurrents along the curve bounding this surface, add up to $n\Phi_0$. Since its initial proposal the LP effect has been measured by several different techniques and several distinct systems, such as a perforated disk with varying hole size[4], a patterned microstructure of an oxide superconductor[5], a single mesoscopic Al ring (SQUID measurement of the susceptibility)[6], an array of Al loops (specific heat measurement)[7], and a single YBCO sub-micron ring[8]. The LP effect can be used to demonstrate many features of the superconducting state, such as the interaction among two superconducting order parameters[9,10] and the study of superconductor/ferromagnet hybrids[11]. The LP effect is well described by the Ginzburg-Landau theory in most of the situations[12–15]. The LP can also exist through fluctuations in the normal phase for very small rings with effective radius $R/\xi < 0.6$ under a constant magnetic field[16].

In this paper we investigate the LP effect in a thin-walled cylinder with a finite height produced by the inhomogeneous magnetic field of a persistent current loop, put on its top. This external magnetic field is that of a magnetic moment pointing along the thin-walled cylinder major axis. In the standard LP effect the height of the thin-walled cylinder plays no role because the applied external field is constant and oriented along the major axis. However in the presence situation the height plays a major role[11]. We report here new features due to the inhomogeneity distribution of the supercurrent in the cylinder, which in its top edge feels a magnetic flux more intense than in the bottom. Our theoretical framework is developed in a current bias regime, which means that the persistent current circulating in the loop is varied and the response of the thin-walled cylinder observed.

The persistent current loop of a (non-superconducting) metallic mesoscopic ring has been observed since decades ago[17] and in principle can be used for an experimental realization of the present proposal. The persistent current loop created by a superconducting mesoscopic ring is another way to realize the present system. In this case the system has two superconductors, for instance, Nb and Al, the former used for the persistent current loop and the latter for the the thin-walled cylinder. Since the Nb critical temperature (T_c = 9.25 K) is 7.8 times larger than that of Al (T_c = 1.18 K)[18], the LP oscillations observed in the thin-walled cylinder are near to the Al transition to the normal state, which happens to fall in the very low temperature domain of the Nb current loop. Therefore the Nb ring generates a stable steady magnetic whose value is swept continuously from zero to its maximum value by varying the persistent current to the maximum Nb critical current. Let a and R be the radii of the external current loop and of the thin-walled cylinder, respectively, as shown in Fig. 1. We

are mostly interested here in the effects brought by the inhomogeneity of the field, and for this reason will concentrate in the case $R > a$. The magnetic moment of the persistent current loop is given by $\mu = I_{loop}\,\pi a^2$ but, notice that the thin-walled cylinder also defines a magnetic moment scale, given by $\mu_0 = \Phi_0\xi_0/2\pi$, where ξ_0 is the zero temperature coherence length of the superconductor that makes the Al thin-walled cylinder. We study the LP oscillations by sweeping the ratio μ/μ_0 to its maximum value μ_c/μ_0. Thus it is of fundamental importance to determine the maximum attained magnetic moment in the current loop, $\mu_c = I_c\,\pi a^2$, I_c being the Nb critical current. According to Sebastien Michotte et al.[19] for T= 1.5 K the Nb critical current is I_c=2000 μA for a wire of width 75 nm. Therefore a ring with radius a=0.5 μm achieves the maximum magnetic moment μ_c=1.5 x 10^{-16} A.m^2. To determine the magnetic moment scale μ_0 of the thin-walled cylinder it suffices to know the zero temperature coherence length of Al. Nanoscopic Al rings have been extensively studied in the literature, such as by Florian R. Ong et al.[7] and Hendrik Bluhm et al.[9]. Data fit in both cases leads to the values of ξ_0 equal to 150 and 70 nm, respectively. Here we shall consider ξ_0=100 nm which gives μ_0=3.2 x 10^{-23}. In summary we find that maximum magnetic moment ratio is μ_c/μ_0=3 x 10^6. Therefore the current circulating in the external loop can be swept up to six orders of magnitude in our suggested system. Notice that our theoretical calculations do not rely in this specific realization which is only a suggested experimental set up for it.

To describe the present system two other lengths must be considered, namely, the distance from the current loop to the center of the thin-walled cylinder, z_1 and the height of the thin-walled cylinder, $Z_0 = 2z_0$, z_0 being the distance from the edge to its center. Throughout this paper the distance between the current loop and the top edge of the thin-walled cylinder is kept fixed and equal to half coherence length, thus $z_1 = 0.5\xi_0 + z_0$. Our analysis is restricted to the thin-walled cylinder, which means that its width is smaller than the coherence length, $w < \xi_0$ and therefore only two coordinates are needed to determine a point in the cylinder, namely, $(\rho = R, \varphi, |z| \leq z_0)$ in cylindrical coordinates with the origin at the center of the thin-walled cylinder. The order parameter inside the thin-walled cylinder is expressed by its phase ϕ and amplitude f, such that $\Psi = f(z)\exp\left(\imath\phi(\varphi, z)\right)$. The well known condition of a single value order parameter implies that $\Psi(\varphi + 2\pi) = \Psi(\varphi)$ and this means that the order parameter must be the same along the z-axis: $\phi = L\varphi$, where L is an integer to be associated with the angular momentum of the vortex state trapped in the thin-walled cylinder. Therefore the order parameter is assumed to have the general form $\Psi(z, \varphi) = f(z)\exp\left(\imath L\varphi\right)$. The dipolar magnetic field falls with the inverse of the cube of the distance to the current loop, thus being strong in the top and weak at the bottom and this will make the amplitude strongly z dependent. Although the current in the external loop always makes the thin-walled cylinder feel a dipolar magnetic field, its inhomogeneity is only noticeable in case the thin-walled cylinder is sufficiently tall. For this reason we numerically study here two examples of thin-walled cylinders here, a short ($Z_0 = 2.0\xi_0$) and a tall ($Z_0 = 10.0\xi_0$) one. The former basically yields standard LP oscillations and the latter comprises novel phenomena because the top and the bottom edges of the thin-walled cylinder are pierced by very distinct magnetic fluxes.

We solve the nonlinear GL equation for the thin-walled



FIG. 1. (Color online) This figure depicts the persistent current loop (radius $a = 5.0\xi_0$) on top of a thin-walled superconducting rod (radius $R = 10.0\xi_0$) put $0.5\xi_0$ away from its edge. Two heights are treated here, corresponding to a short ($Z_0 = 2.0\xi_0$) and a tall ($10.0\xi_0$)cylinder.

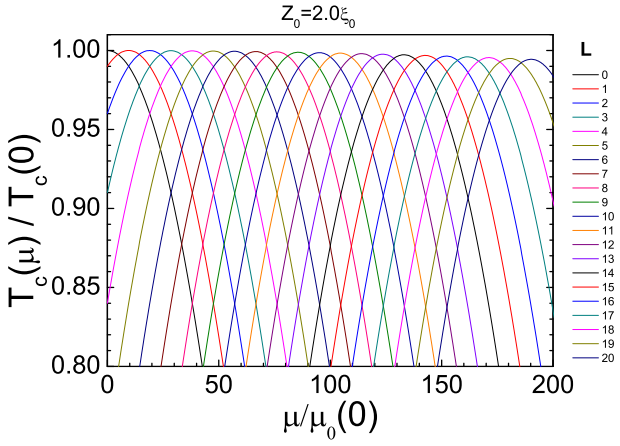


FIG. 2. (Color online) The LP temperature $T_c(\mu)$ versus the magnetic moment μ is shown here for the short cylinder (height $Z_0 = 2.0\xi_0$). The L lines, ranging from 0 to 20, are obtained from the linear theory (Eq.(13)) and describe angular momenta trapped in the cylinder.

cylinder through the finite element method (COMSOL and MATLAB softwares) and check that our numerical procedure is correct in the short cylinder limit, since in this case, we also solve the theory analytically. This gives confidence that our numerical results for the thin-walled cylinder are reliable.

The paper is organized as follows. In section II we review the basic Ginzburh-Landau formalism applied to the thin-walled cylinder in present of a persistent current loop. In section III we explore the limit that the amplitude f can be considered as constatn along the height to obtain important theorems relating the zero current to the minimum of the free energy. In section IV we numerically study the short and tall cylinders and find that the latter displays two distinct regimes according to the the value of the persistent current. Finally in section V we reach some conclusion about the results obtained here.

II. THEORETICAL BACKGROUND

The Ginzburg-Landau theory describes the superconductor near to its critical temperature T_c. Because the London penetration length is taken to be much larger than the hollow cylinder height, the shielding of the magnetic field is safely ignored in our calculations. Hence the free energy density is simply that of the sum of terms involving the order parameter:

$$\mathcal{F} = \int_\Omega d\upsilon \Big[\frac{\hbar^2}{2m} \Big| \Big(\vec{\nabla} - \frac{2\pi i}{\Phi_0} \vec{A} \Big) \Psi \Big|^2 + \alpha(T) |\Psi|^2 + \frac{\beta}{2} |\Psi|^4 \Big] \tag{1}$$

where $\alpha(T) \equiv \alpha_0 \Big(\frac{T}{T_c} - 1 \Big)$, therefore $\alpha(T) \leq 0$ to sustain the superconducting state, and β is a constant. The volume of the thin-walled cylinder is $\Omega \equiv 2\pi R w Z_0$ and the dimensionless volume element is $d\upsilon \equiv d^3x/\Omega$. From the variational principle one obtains the Ginzburg-Landau equation that determines the order parameter which minimizes this free energy:

$$-\frac{\hbar^2}{2m} \Big(\vec{\nabla} - \frac{2\pi i}{\Phi_0} \vec{A} \Big)^2 \Psi = -\alpha(T)\Psi + \beta |\Psi|^2 \Psi \tag{2}$$

The persistent current loop has its center located at coordinates $(0, 0, z_1)$, its magnetic moment is $\mu = I_{loop} \pi a^2$, I_{loop} being the circulating current. The vector potential describing its field in space is given by $\vec{A}(\rho, z) = A_\varphi(\rho, z) \hat{\varphi}$[20],

$$\begin{aligned} A_\varphi(\rho, z) &\equiv \frac{\mu \rho}{[\rho^2 + a^2 + (z - z_1)^2]^{3/2}} \cdot \\ &\cdot \sum_{n=0}^{\infty} \frac{(4n+1)!!}{2^{2n} n! (n+1)!} \Big(\frac{a\rho}{\rho^2 + a^2 + (z - z_1)^2} \Big)^{2n} = \\ &= \frac{\mu \rho}{[\rho^2 + a^2 + (z - z_1)^2]^{3/2}} \Big\{ 1 + \frac{15}{8} q^2 + \frac{315}{64} q^4 + \cdots \Big\}, \\ q &= \frac{a\rho}{\rho^2 + a^2 + (z - z_1)^2}. \end{aligned} \tag{3}$$

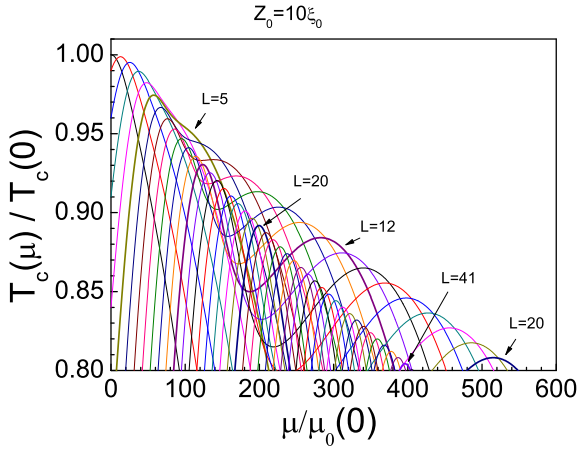


FIG. 3. (Color online) The LP temperature $T_c(\mu)$ versus the magnetic moment μ is shown here for the tall cylinder (height $Z_0 = 10.0\xi_0$). The L lines, ranging from 0 to 41, are obtained from the linear theory (Eq.(13)) and describe angular momenta states trapped in the cylinder. A few selected curves are shown as thick lines and their properties discussed in the text.

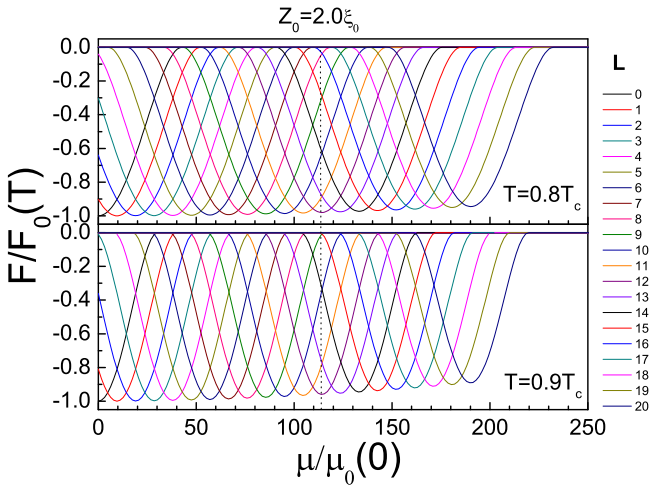


FIG. 4. (Color online) The free energy of the short cylinder (height $Z_0 = 2.0\xi_0$) is shown here for two temperatures $T = 0.8T_c$ and $T = 0.9T_c$. Free energy L lines ranging from 0 to 20 are shown versus the magnetic moment μ of the persistent current loop. A dashed vertical line indicates that the position of the minima is approximately the same for the two temperatures.

The thin-walled condition restricts the radial coordinate to $\rho = R$, and so, it suffices to use the expression,

$$A_\varphi(R,z) = \frac{\mu}{R^2}\eta(z), \quad \text{where} \tag{4}$$

$$\eta(z) \equiv \frac{1}{\left[1+\left(\frac{a}{R}\right)^2+\left(\frac{z-z_1}{R}\right)^2\right]^{3/2}}\big(1+1.8750p^2+$$
$$+4.9219p^4+14.6631p^6+46.7386p^8+155.4058p^{10}+$$
$$+531.8949p^{12}+1.8593\,10^3p^{14}+6.6042\,10^3p^{16}+$$
$$+2.3757\,10^4p^{18}+8.6335\,10^4p^{20}+\cdots\big) \tag{5}$$

$$p = \frac{\frac{a}{R}}{1+\left(\frac{a}{R}\right)^2+\left(\frac{z-z_1}{R}\right)^2}. \tag{6}$$

A term $c_{2n}\,p^{2n}$ of this series expansion has the coefficient c_{2n} growing with n, as shown above, that must be overcome by p^{2n} in order to achieve convergency. For instance, in the present case of interest, $R = 10.0\xi_0$, $a = 5.0\xi_0$, and we take the top edge of the cylinder, $z - z_1 = -0.5\xi_0$ to obtain that $p = 0.3992$. Precision of the order 10^{-3} is only achieve near the $n = 10$ term when $c_{20} = 8.6335\,10^4$ times $p^{20} = 1.05\ 10^{-8}$ gives $c_{20}\,p^{20} = 9.0651\,10^{-4}$.

It is worthwhile to compute the magnetic flux that pierces a ring resulting from the intersection of the thin-walled cylinder with a plane z:

$$\Phi(\mu,z) \equiv \oint_z d\vec{l}\cdot\vec{A}(R,z) =$$
$$= 2\pi R A_\varphi(R,z) = \frac{2\pi\mu}{R}\eta(z) \tag{7}$$

$$\frac{\Phi(\mu,z)}{\Phi_0} = \frac{\mu}{\mu_0}\frac{\xi_0}{R}\eta(z) \tag{8}$$

Eq.(8) shows that the ratio between the magnetic moments, μ/μ_0, together with the geometrical parameters, defines the ratio between the z plane magnetic flux and the fundamental flux. In order to gain insight into this series expansion, let us analyze it in the case treated here, namely, the ratio between the current loop and the thin-walled cylinder radii is equal to one half, $a/R = 0.5$. Suppose a point at the surface of the thin-walled cylinder near to its top, such that $(z - z_1)/R \approx 0$. In this case we have that $p^2 \approx 0.16$ and $1+\frac{15}{8}p^2+\frac{315}{64}p^4+\cdots \approx 1+0.30+0.12+\cdots$. We learn that the series terms contribute in this example, although they do not add any significant qualitative change if instead we had considered the point like dipole limit $a \to 0$. Thus in this limit all the corrections in powers of $(a/R)^2$ do not exist and the field is that of a point like magnetic dipole, $\vec{\mu} = \mu\hat{z}$ given by $\vec{A} = \vec{\mu}\times\vec{r}/|\vec{r}|^3$ where $\vec{r} = R\hat{\rho}+(z-z_1)\hat{z}$ falls in the surface of the thin-walled cylinder.

We write the order parameter in terms of its amplitude f and phase $\phi = L\varphi$ to obtain the following expression for the kinetic energy in terms of the geometry, the angular momentum L and the vector potential A_φ:

$$G \equiv \frac{\hbar^2}{2m}\int_\Omega dv\Big\{\Big(\frac{\partial f}{\partial z}\Big)^2+\frac{1}{R^2}\Big[L-\frac{\Phi(\mu,z)}{\Phi_0}\Big]^2 f^2\Big\} \tag{9}$$

Then the free energy density becomes,

$$\mathcal{F} = G + \int_\Omega dv\Big[-\alpha(T)f^2+\frac{\beta}{2}f^4\Big] \tag{10}$$

We also write the supercurrent density, $\vec{J} \equiv \frac{q\hbar}{m}\Im\Big[\Psi^*\Big(\vec{\nabla}-\frac{2\pi i}{\Phi_0}\vec{A}\Big)\Psi\Big]$, in terms of the amplitude and the phase de-

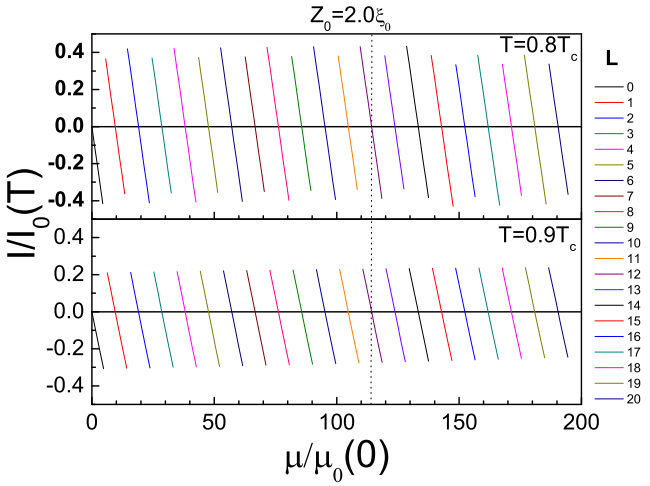


FIG. 5. (Color online) The current circulating in the short cylinder (height $Z_0 = 2.0\xi_0$) is shown here for two temperatures $T = 0.8T_c$ and $T = 0.9T_c$. Current L lines ranging from 0 to 20 are shown versus the magnetic moment μ of the persistent current loop. A dashed vertical line indicates that the vanishing of the current is approximately the same for the two temperatures.

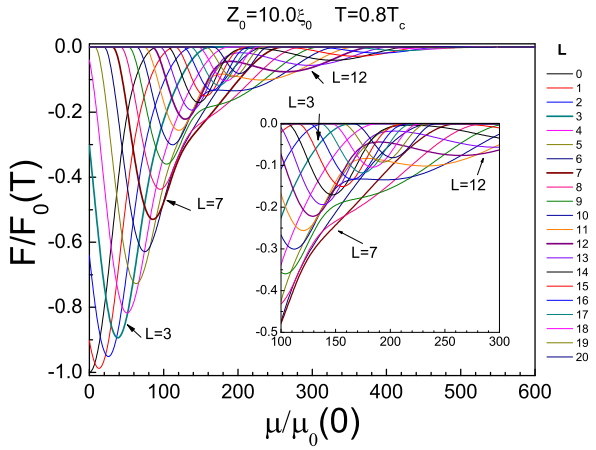


FIG. 6. (Color online) The free energy of the tall cylinder (height $Z_0 = 10.0\xi_0$) is shown here for the temperature $T = 0.8T_c$. Free energy L lines ranging from 0 to 20 are shown versus the magnetic moment μ of the persistent current loop. Some L states are depicted as thick lines to exemplify the three existing regimes: single well ($L = 3$), transition ($L = 7$), and double well ($L = 12$). The inset helps to visualize the transition regime.

composition using the cylindrical symmetry:

$$\vec{J} = \frac{q\hbar}{mR}[f(z)]^2\Big[L - \frac{\Phi_0(\mu,z)}{\Phi_0}\Big]\hat{\varphi}. \tag{11}$$

There has been many proposed methods to calculate the current of the LP effect[21,22]. In our numerical calculations the current circulating in the thin-walled cylinder is simply obtained as an integration of the current density, $\vec{J}$, along the cross-section of the cylinder. According to the thin-walled condition $w \sim \xi_0$, and so,

$$\begin{aligned} I &= w\int_{-z0}^{z0} dz\vec{J}\cdot\hat{\varphi} = \\ &= I_0\int_{-z0}^{z0}\frac{dz}{Z_0}\Big[\frac{f(z)}{\sqrt{\alpha_0/\beta}}\Big]^2\Big[L - \frac{\Phi(\mu,z)}{\Phi_0}\Big], \end{aligned} \tag{12}$$

in terms of the current parameter $I_0 \equiv \big(q\hbar Z_0 w\alpha_0\big)/\big(m\beta R\big)$. The LP oscillations occur near to the critical temperature, where the order parameter is weak, and so, besides the non-linear, the linear version of Eq.(2), with the cubic term neglected, can be used. Then there is a Schrödinger like equation for the amplitude $f(z)$, once the order parameter is taken as $\Psi(z,\varphi) = f(z)\exp\big(\imath L\varphi\big)$:

$$\Big[-\frac{\hbar^2}{2m}\frac{d^2}{dz^2} + V(z)\Big]f(z) = -\alpha(T)f(z), \tag{13}$$

where the potential is given by

$$V(z) = \frac{\hbar^2}{2mR^2}\Big[L - \frac{\Phi(\mu,z)}{\Phi_0}\Big]^2, \tag{14}$$

and the boundary condition at the edges of the thin-walled cylinder are $df(z)/dz|_{(z=\pm z_0)} = 0$, which is automatically satisfied in the limit of a constant f. Let us consider the ill-defined limit, but still instructive, of f z independent, such that $d^2f(z)/dz^2 \approx 0$. Then the above equation defines a condition under the simple assumption that there is a non-zero f: $V(z) + \alpha(T) = 0$ or equally, $T/T_c = 1 - \big(\xi_0/R\big)^2\big[L - \Phi(\mu,z)/\Phi_0\big]^2$. This defines the LP temperature, which is a function of the flux that pierces the thin-walled cylinder along the z plane. However because $\Phi(\mu,z)$ is z dependent, the found ratio T/T_c is in contradiction with the original argument. Indeed a z independent amplitude f is only possible for a very short thin-walled cylinder, and this entitles us to take $z = 0$, which means the medium plane. We choose to express the above ratio T/T_c in terms of the $T = 0$ coherence length, $\xi_0 \equiv \sqrt{\hbar^2/2m\alpha_0}$. The dimensionless ratio $\Phi(\mu,z)/\Phi_0$ can be written in terms of the dimensionless length ratios, R/ξ_0, a/R, and $(z - z_1)/R$, and the dimensionless magnetic moment ratio, μ/μ_0 where μ_0 has been previously defined. This naive approach to the LP oscillations is improved in the next sections by treating the z dependence of this problem. The thin-walled cylinder in presence of the inhomogeneous field produced by the persistent current loop field makes the amplitude dependent on its height position: $f(z)$. In this case we also solve the above Schröedinger equation in order to determine $f(z)$.

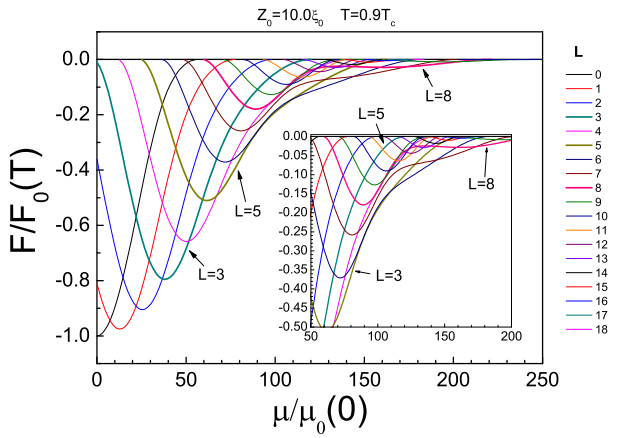


FIG. 7. (Color online) The free energy of the tall cylinder (height $Z_0 = 10.0\xi_0$) is shown here for the temperature $T = 0.9T_c$. Free energy L lines ranging from 0 to 18 are shown versus the magnetic moment μ of the persistent current loop. Some L states are depicted as thick lines to exemplify the three existing regimes: single well ($L = 3$), transition ($L = 5$), and double well ($L = 8$). The inset helps to visualize the transition regime.

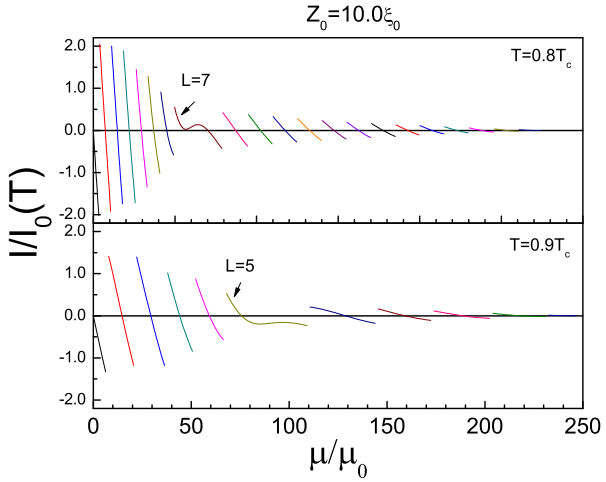


FIG. 8. (Color online) The current circulating in the tall cylinder (height $Z_0 = 10.0\xi_0$) is shown here for the temperatures $T = 0.8T_c$ and $T = 0.9T_c$. Current L lines ranging are shown versus the magnetic moment μ of the persistent current loop for the L values of Figs.(6) and (7). The single and double well regimes reflect in current lines with different slopes and the two regimes are separated by a transition line, $L = 7$ for $T = 0.8T_c$, and $L = 5$ for $T = 0.9T_c$, respectively.

III. THE RING LIMIT

A thin-walled cylinder such the order parameter amplitude f is constant along the z direction, and therefore $\partial f/\partial z = 0$, we define as a ring. The validity of the ring treatment restricts the height to a few coherence length units, which means that the ratio z_0/ξ_0 cannot be very large. In the ring limit all that is necessary to determine the order parameter and the free energy is to compute the integrals,

$$g(\mu) \equiv \int_{-z0}^{z0} \frac{dz}{Z_0}\Big[L - \frac{\Phi(\mu,z)}{\Phi_0}\Big]^2, \quad \text{and,} \tag{15}$$

$$g'(\mu) \equiv \int_{-z0}^{z0} \frac{dz}{Z_0}\Big[L - \frac{\Phi(\mu,z)}{\Phi_0}\Big]. \tag{16}$$

The kinetic energy energy becomes $G = \alpha_0\big(\frac{\xi_0}{R}\big)^2 g f^2$ and the current $I = \frac{q\hbar}{m}\frac{wZ_0}{R} f^2 g'$. Then, we have for the free energy,

$$\mathcal{F} = [\alpha_0\big(\frac{\xi_0}{R}\big)^2 g + \alpha(T)]f^2 + \frac{\beta}{2}f^4 \tag{17}$$

whose minimization determines the order parameter and its minimum:

$$f^2 = -\frac{1}{\beta}\big[\alpha_0\big(\frac{\xi_0}{R}\big)^2 g + \alpha(T)\big]$$

$$\mathcal{F} = -\frac{1}{\beta}\big[\alpha_0\big(\frac{\xi_0}{R}\big)^2 g + \alpha(T)\big]^2 \tag{18}$$

Notice that since $g > 0$ and the above equation determines that $\alpha_0\big(\frac{\xi_0}{R}\big)^2 g + \alpha(T) \leq 0$ because $f_0^2 > 0$ then there is a temperature bound given by $\alpha(T) \leq -\alpha_0\big(\frac{\xi_0}{R}\big)^2 g$. The upper bond defines the LP temperature, which corresponds to the vanishing of the order parameter, such that the superconductor reaches the normal state for a temperature which depends on g and the α_0 parameter, according to the above equation. Therefore the LP oscillations obtained from the non-linear theory in case of f constant are expressed in terms of the integrals g and g'. The corresponding free energy, current and critical temperature are defined as follows:

$$\mathcal{F}(\mu,T) = -\mathcal{F}_0\Big[\frac{T - T_c(\mu)}{T_c}\Big]^2 \tag{19}$$

$$\frac{T_c(\mu)}{T_c} = 1 - \big(\frac{\xi_0}{R}\big)^2 g(\mu) \tag{20}$$

$$I(\mu,T) = -I_0\Big[\frac{T - T_c(\mu)}{T_c}\Big] g'(\mu) \tag{21}$$

The integrals $g(\mu)$ and $g'(\mu)$ can be expressed in terms of the following defined integrals:

$$\langle L\rangle \equiv \int_{-z0}^{z0} \frac{dz}{Z_0}\frac{\Phi(\mu,z)}{\Phi_0}, \quad \text{and,} \tag{22}$$

$$\langle L^2\rangle \equiv \int_{-z0}^{z0} \frac{dz}{Z_0}\Big(\frac{\Phi(\mu,z)}{\Phi_0}\Big)^2, \tag{23}$$

such that, the two integrals can be written as,

$$\langle L\rangle = \frac{\mu}{\mu_0} I_1, \quad I_1 \equiv \frac{\xi_0}{R}\int_{-z0}^{z0} \frac{dz}{Z_0}\eta(z), \quad \text{and,} \tag{24}$$

$$\langle L^2\rangle = \big(\frac{\mu}{\mu_0}\big)^2 I_2, \quad I_2 \equiv \big(\frac{\xi_0}{R}\big)^2 \int_{-z0}^{z0} \frac{dz}{Z_0}\big[\eta(z)\big]^2 \tag{25}$$

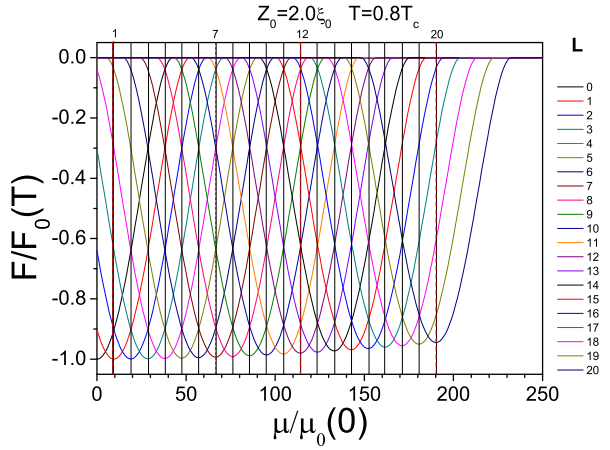


FIG. 9. (Color online) Vertical lines associated to the vanishing of the current are plotted together with the free energy for the short cylinder (height $Z_0 = 2.0\xi_0$) at the temperature $T = 0.8T_c$. L states ranging from 0 to 20 are considered here. The μ values equal to 9.62, 66.64, 114.04 and 190.29, labeled as (1), (7), (12) and (20), respectively, are depicted as red dashed vertical lines and are selected for further analysis in Fig.(11).

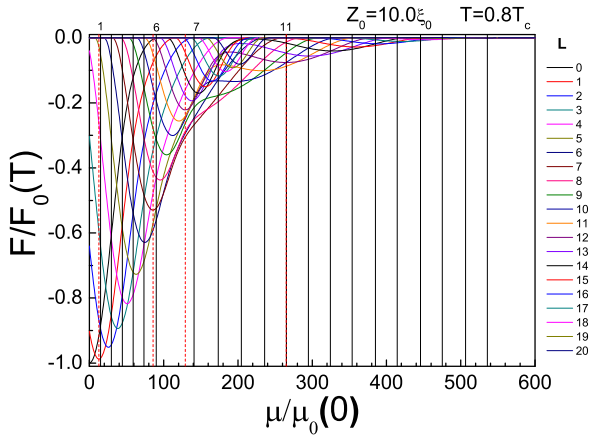


FIG. 10. (Color online) Vertical lines associated to the vanishing of the current are plotted together with the free energy for the tall cylinder (height $Z_0 = 10.0\xi_0$) at the temperature $T = 0.8T_c$. L states ranging from 0 to 20 are considered here. The μ values equal to 12.75, 85.64, 129.02 and 264.97, labeled as (1), (6), (7) and (11), respectively, are depicted as red dashed vertical lines and are selected for further analysis in Fig.(12).

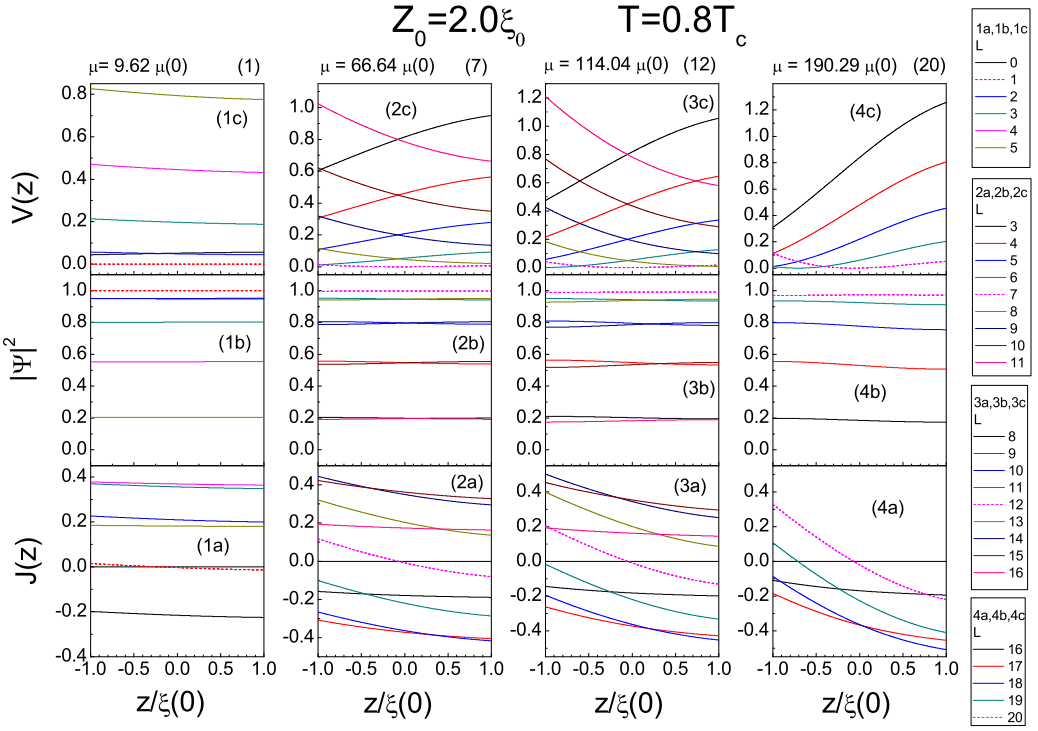


FIG. 11. (Color online) The current density J, the pair density $|\psi|^2$ and the potential V of the linear equation (Eq.(44)), along the cylinder height are shown here for the short cylinder (height $Z_0 = 2.0\xi_0$) at the temperature of $T = 0.8T_c$. The μ values, selected in Fig.(9), and equal to 9.62, 66.64, 114.04 and 190.29, labeled as (1), (7), (12) and (20), are considered for this purpose. The persistent current loop is located at position $1.5\xi_0$. The L lines and their corresponding figures are also listed here.

By taking that $\left(\frac{\xi_0}{R}\right)^2 \int_{-z0}^{z0} \frac{dz}{Z_0}\left[\eta(z) - I_1\right]^2 \geq 0$, we obtain that

$$I_2 - I_1^2 \geq 0. \tag{26}$$

Next we show three important features of the LP oscillations with respect to the magnetic moment μ that can be expressed in terms of the above functions $g(\mu)$ and $g'(\mu)$, written in the following way:

$$g(\mu) = L^2 - 2L\frac{\mu}{\mu_0}I_1 + \left(\frac{\mu}{\mu_0}\right)^2 I_2, \quad \text{and,} \tag{27}$$

$$g'(\mu) = L - \frac{\mu}{\mu_0}I_1. \tag{28}$$

These three three features are valid to all temperatures, and for this reason assume that $T \neq T_c(\mu)$. They are associated to three special moments, μ_f, μ_c and μ_t, defined as such:

1) *The minimum of the free energy.* According to Eq.(19), $\partial\mathcal{F}/\partial\mu = 0$ is the same condition as the minimum with respect to the critical temperature, $\partial T_c(\mu)/\partial\mu = 0$, which boils down to $\partial g(\mu)/\partial\mu = 0$. This defines the magnetic moment μ_f.

$$\frac{\mu_f}{\mu_0} = L\frac{I_1}{I_2} \tag{29}$$

2) *The vanishing of the current.* According to Eq.(21) the condition $I(\mu) = 0$ happens for $g'(\mu) = 0$. This defines the magnetic moment μ_c:

$$\frac{\mu_c}{\mu_0} = L\frac{1}{I_1} \tag{30}$$

3) *The highest LP temperature.* According to Eq.(20) this occurs when the LP temperature becomes the critical one. However the condition $Tc(\mu)/T_c = 1$ is the same as $g(\mu) = 0$. This defines the magnetic moment μ_t:

$$\frac{\mu_t}{\mu_0} = L\frac{I_1}{I_2}\left(1 \pm \imath\sqrt{\frac{I_2}{I_1^2} - 1}\right) \tag{31}$$

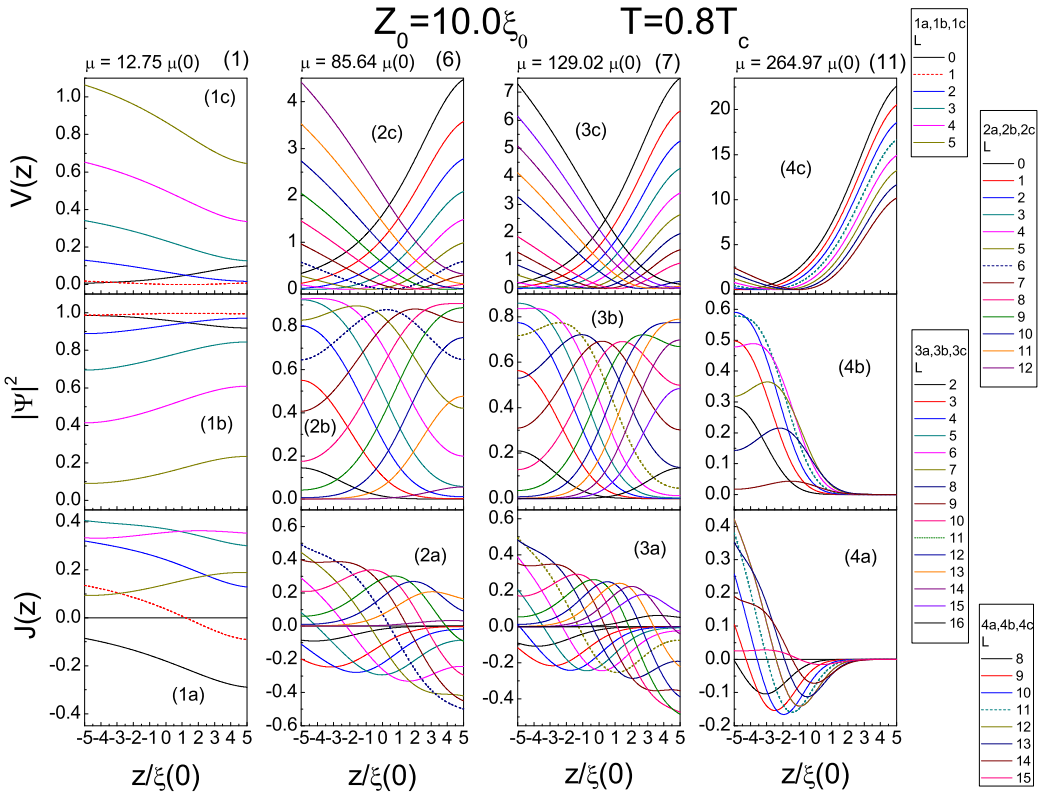


FIG. 12. (Color online) The current density J, the pair density $|\psi|^2$ and the potential V of the linear equation (Eq.(44)), along the cylinder height are shown here for the tall cylinder (height $Z_0 = 10.0\xi_0$) at the temperature of $T = 0.8T_c$. The μ values, selected in Fig.(10), and equal to 12.75, 85.64, 129.02 and 264.97, labeled as (1), (6), (7) and (11), are considered for this purpose. The persistent current loop is located at position $5.5\xi_0$. The L lines and their corresponding figures are also listed here.

Then we prove that *the LP temperature never reaches the critical temperature* T_c, unless for the zero height ring, where $\Phi_0(\mu, z) = \Phi_0(\mu, 0)$ $(I_2 = I_1^2)$. Notice that

$$\frac{\mu_c}{\mu_f} = \frac{I_2}{I_1^2} \geq 1, \tag{32}$$

which means that *the current in the thin-walled cylinder always vanishes after the free energy reaches its minimum* $(\mu_c \geq \mu_f)$ by increasing the current in the loop. Another important aspect to consider is that the three special magnetic moments, defined by Eqs.(29), (30) and (31), are temperature independent. This means that *the distance between two consecutive* L *and* $L+1$ *magnetic moments, either free energy minima or zeros of the current, are temperature independent and equal to* I_1/I_2 *and* $1/I_1$, respectively. For a very short ring, defined to have height comparable to the coherence length, $Z_0 \leq \xi_0$, the integrals I_1 and I_2 are easily computed, since it is enough to take the integrands at the center of the ring, $z \approx 0$, to obtain that $I_1 \approx \eta(0)$, and $I_2 \approx \eta(0)^2$. The three conditions, namely, the minimum of the free energy, the vanishing of the current and the highest LP temperature take place at the same point $\mu/\mu_0 = L/I_1$ because $I_1^2 = I_2$. Inserting the integrals and using the magnetic flux definition of Eq.(7) in the center plane of the ring we obtain for the free energy density, critical temperature and current density the following expressions:

$$\mathcal{F}(\mu, T) = -\mathcal{F}_0 \Big[\frac{T - T_c(\mu)}{T_c}\Big]^2 \tag{33}$$

$$\frac{T_c(\mu)}{T_c} \equiv 1 - \Big(\frac{\xi_0}{R}\Big)^2 \Big[L - \frac{\Phi(\mu, 0)}{\Phi_0}\Big]^2 \tag{34}$$

$$I(\mu, T) = -I_0 \Big[\frac{T - T_c(\mu)}{T_c}\Big]\Big[L - \frac{\Phi(\mu, 0)}{\Phi_0}\Big] \tag{35}$$

$$\tag{36}$$

where we have defined the parameters, associated to the free energy, $\mathcal{F}_0 \equiv \alpha_0^2/\beta$, and to the current, I_0, previously defined. Notice that the above LP temperature was previously obtained using the linear approach. The above case is the standard LP effect. valid for a constant applied external field and arbitrary height.

To show how the height of the cylinder affects the LP oscillations we discuss below the approximation that f is still a constant, but the integrals g and g' must be integrated along the z axis. We get analytical insight into

this problem by taking that the current loop is very small as compared to the thin-walled cylinder, $a/R << 1$, such that just the first term of the series expansion given in Eq.(4) is enough to describe the external magnetic field:

$$\eta(z) = \frac{1}{[1+\left(\frac{z-z_1}{R}\right)^2]^{3/2}}. \tag{37}$$

This vector potential is introduced into Eqs.(15) and (16) to obtain that,

$$I_1 = \frac{\xi_0}{Z_0}\{\frac{\left(\frac{z_0-z_1}{R}\right)}{\sqrt{1+\left(\frac{z_0-z_1}{R}\right)^2}} + \frac{\left(\frac{z_0+z_1}{R}\right)}{\sqrt{1+\left(\frac{z_0+z_1}{R}\right)^2}}\} \tag{38}$$

$$\begin{aligned} I_2 = \frac{\xi_0^2}{Z_0 R}\{\frac{1}{4}[\frac{\left(\frac{z_0-z_1}{R}\right)}{\left(1+\left(\frac{z_0-z_1}{R}\right)^2\right)^2} + \frac{\left(\frac{z_0+z_1}{R}\right)}{\left(1+\left(\frac{z_0+z_1}{R}\right)^2\right)^2}] + \\ + \frac{3}{8}[\frac{\left(\frac{z_0-z_1}{R}\right)}{1+\left(\frac{z_0-z_1}{R}\right)^2} + \frac{\left(\frac{z_0+z_1}{R}\right)}{1+\left(\frac{z_0+z_1}{R}\right)^2}] + \\ + \frac{3}{8}[\arctan\left(\frac{z_0-z_1}{R}\right) + \arctan\left(\frac{z_0+z_1}{R}\right)]\} \end{aligned} \tag{39}$$

These integrals are expanded in a Taylor series in powers of $(z_0/R)^2$, which is a small parameter, since the approximation of f constant is a good one only for a short cylinder. We obtain for the integrals I_1 and I_2 the following values by keeping contributions of lowest order $(z_0/R)^2$ and neglecting higher ones.

$$\begin{aligned} I_1 &= \frac{\xi_0}{R}\frac{1}{\left[1+\left(\frac{z_1}{R}\right)^2\right]^{3/2}}\{1-\frac{1}{2}\frac{1-4\left(\frac{z_1}{R}\right)^2}{\left[1+\left(\frac{z_1}{R}\right)^2\right]^2}\left(\frac{z_0}{R}\right)^2\} \\ I_2 &= \left(\frac{\xi_0}{R}\right)^2\frac{1}{\left[1+\left(\frac{z_1}{R}\right)^2\right]^3}\{1-\frac{1-7\left(\frac{z_1}{R}\right)^2}{\left[1+\left(\frac{z_1}{R}\right)^2\right]^2}\left(\frac{z_0}{R}\right)^2\} \end{aligned} \tag{40}$$

We notice that the above equations do satisfy the inequality of Eq.(26),

$$I_2 - I_1^2 = 3\frac{\left(\frac{\xi_0}{R}\right)^2\left(\frac{z_0}{R}\right)^2\left(\frac{z_1}{R}\right)^2}{\left[1+\left(\frac{z_1}{R}\right)^2\right]^5} \tag{41}$$

As an example let us consider the short cylinder with radius $R = 10.0\xi_0$, half-height $z_0 = 1.0\xi_0$ and the current loop just above its top, $z_1 = 1.5\xi_0$. Then $I_2 - I_1^2 \sim \left(\frac{\xi_0}{R}\right)^2\left(\frac{z_0}{R}\right)^2\left(\frac{z_1}{R}\right)^2 \sim 10^{-6}$. The distance between two consecutive free energy minima is $10.2456\mu_0$ and between two consecutive current zeros is $10.3507\mu_0$.

IV. NUMERICAL ANALYSIS

We obtain numerical solutions of the non-linear GL equation below,

$$\left[-\frac{\hbar^2}{2m}\frac{d^2}{dz^2} + V(z)\right]f(z) = -\alpha(T)f(z) + \beta f(z)^3. \tag{42}$$

by solving it through the finite element method (COMSOL and MATLAB softwares). Then we obtain the free energy, the current density and the current from Eqs.(1), (11), and (12), respectively, by input of $f(z)$, obtained from Eq.(42).

To obtain the numerical solutions of Eq.(42) we cast it in dimensionless quantities, represented by a bar on top of the corresponding variable: $\bar{f} = \sqrt{\beta/\alpha(T)}f$, $\bar{z} = z/\xi(T)$, where $\xi(T) = \xi_0/\sqrt{1-T/T_c}$, and $\bar{V} = V/\alpha(T)$. The explicit temperature dependence disappears from Eq.(42) which becomes,

$$\left[-\frac{d^2}{d\bar{z}^2} + \bar{V}(\bar{z})\right]\bar{f}(\bar{z}) = -\bar{f}(\bar{z}) + \bar{f}(\bar{z})^3. \tag{43}$$

In practical grounds this means that all the lengths are measured in units of $\xi(T)$, the temperature dependent coherence length, and so, ratios between two lengths become temperature independent. For instance, the function η, defined by Eq.(5), is found to be temperature independent, $\eta(\bar{z}) = \eta(z)$, since it only depends on ratios. The dimensionless version of the potential, defined in Eq.(44), becomes temperature dependent and given by,

$$\bar{V}(\bar{z}) = \frac{1}{\bar{R}(T)^2}\left[L - \bar{\mu}(T)\frac{\eta(\bar{z})}{\bar{R}(T)}\right]^2. \tag{44}$$

where $\bar{R}(T) = R/\xi(T)$, $\bar{\mu}(T) = \mu/\mu_0(T)$ and $\mu_0(T) = \Phi_0\xi(T)/2\pi$. Notice that the product $\mu_0(T)\bar{R}(T) = \Phi_0 R/2\pi$ is temperature independent. Like the radius, the height of the cylinder also shrinks to zero as T approaches T_c: $\bar{z}_0 = z_0/\xi(T)$.

The free energy, the current density and the current, obtained from Eqs.(1), (11), and (12), respectively, by input of $f(z)$, determined from Eq.(42), are also cast into dimensionless units. The current is given by,

$$\bar{I} = \int_{-\bar{z}_0}^{\bar{z}_0}\frac{d\bar{z}}{\bar{Z}_0}\,\bar{f}(\bar{z})^2\left[L - \bar{\mu}(T)\frac{\eta(\bar{z})}{\bar{R}(T)}\right] \tag{45}$$

where $\bar{I} = I/I_0(T)$, $I_0(T) \equiv \left(q\hbar\bar{Z}_0 w\alpha(T)\right)/\left(m\beta\bar{R}\right)$. The free energy in reduced units becomes,

$$\bar{F} = \int_{-\bar{z}_0}^{\bar{z}_0}\frac{d\bar{z}}{\bar{Z}_0}\left\{\left[\frac{d\bar{f}(\bar{z})}{d\bar{z}}\right]^2 + \left[\bar{V}(\bar{z}) - 1\right]\bar{f}(\bar{z})^2 + \frac{1}{2}\bar{f}(\bar{z})^4\right\} \tag{46}$$

where $\bar{F} = F/F_0(T)$, $F_0(T) \equiv \alpha(T)^2/2\beta$.

We concentrate our numerical study in two thin walled cylinders, both with the same radius $R = 10.0\xi_0$ in presence of the same current loop ring with radius $a = 5.0\xi_0$, set at $0.5\xi_0$ above the top edge. The two cylinders only differ by the height, taken to be $Z_0 = 2.0\xi_0$ and $Z_0 = 10.0\xi_0$, such that $z_1 = 1.5\xi_0$ and $5.5\xi_0$, respectively. We apply the same numerical method to both, but the short cylinder is expected to have the amplitude f nearly z independent and be approximately described by the analytical ring limit previously considered. From the other side the tall cylinder, $Z_0 = 10.0\xi_0$, can only be

described by the full numerical treatment since the amplitude varies along the cylinder's height, $f(z)$. All the free energy and the current plots are in terms of the $T = 0$ magnetic moment $\mu/\mu_0(0)$, in order to have a temperature independent scale. Notice that $\mu_0(T) = \Phi_0\xi(T)/2\pi$ and we are taking its zero temperature value as our magnetic moment scale.

Figs. (2) and (3) show the LP temperature versus magnetic moment temperature diagram derived from the linear theory. The ratio $T_c(\mu)/T_c$ is calculated from the lowest eigenvalue of Eq.(43) and (14) for given L and $\mu/\mu_0(0)$ values. These L lines set the border line that separates the superconducting to the normal state in the diagram. The two cylinders display very distinct $T_c(\mu)/T_c$ versus $\mu/\mu_0(0)$ curves, as shown in Figs. (2) and (3).

Fig. (2) covers the 0 to 200 $\mu/\mu_0(0)$ range, which contains the first 20 L lines of the $Z_0 = 2\xi_0$ cylinder. Notice the parabolic shape of the L lines and their nearly homogeneous spatial distribution. The distance between two consecutive maxima, of L and $L + 1$ lines, is described by the formula $\Delta\mu/\mu_0(0) \approx 9.5$. Notice that for increasing magnetic moment the ratio $T_c(\mu)/T_c$ becomes lower than one, indicating that the height of the cylinder matters in this case, and our theoretical considerations developed in the ring limit applies to this situation and is determined by Eq.(20) and not by Eq.(34). The ratio $T_c(\mu)/T_c$ reaches one only in case there is only a single magnetic flux piercing the ring, that is, in case of the nearly zero height cylinder or of the constant magnetic field applied to cylinder of a arbitrary height.

Fig. 3 shows a much richer structure for the L lines of the $R = 10\xi_0$ cylinder, due to the inhomogeneity of the magnetic field that results in distinct magnetic fluxes piercing this cylinder, each for a different z plane intersect. Notice the presence of an inner and an external (true) border lines. To understand the $R = 10\xi_0$ diagram, we selected a few L lines, plotted as thick lines for best visualization purposes: $L = 5$, 12, 20 and 41. The $L = 12$ line is a key case because of its double peak structure with a local minimum between them, a common feature to many lines. The first peak is narrow and tall, while the second peak is short and broad and takes place at a larger magnetic moment than the first peak. The tips of the narrow and broad peaks of the $L = 20$ line still fall inside the plotted temperature range, 0.8 to 1.0 $T_c(\mu)/T_c$. The $L = 5$ thick line shows the onset of the second peak, not present in the lower L lines, which only have a single peak. The $L = 5$ and 6 can be regarded as transition lines to the onset of the second peak and $L = 7$ is the critical line because the second peak is clearly established for $L = 8$ and beyond. $L = 41$ is the highest line in this diagram, seen around $\mu/\mu_0(0) = 400$ and setting the end of an inner transition line inside the superconducting region. The first (narrow) peak contributes to the true border line only up to $L = 4$ then to submerge and form an inner border line for high L values. Thus this inner border line is the curve tangent to the maximum of the first peaks. From its side, the second (broad) peak only contributes to the true superconducting normal state border line, from the $L = 5$ line up to $L = 20$ line. For the sake of the argument we have included the $L = 5, 6$ and 7 lines in this set, although the second peak is only in an embryonic level there. In conclusion the superconducting normal state border line has less angular momentum states for the tall cylinder, since $L = 20$ is the maximum possible value reached at $\mu/\mu_0 = 510$, whereas for the short cylinder, $L = 20$ is reached for $\mu/\mu_0 = 200$.

The full non-linear theory is used to obtain the next plots, which means that Eq.(43) is numerically solved by means of the finite element method, and next the free energy and current calculated from Eqs.(46) and (45), respectively. In the dimensionless treatment the temperature T is introduced by adjustment of the radius and of the height, given by $\bar{R}(T)$ and $\bar{Z}_0(T)$, respectively.

Fig. 4 shows several L free energy lines of the $Z_0 = 2.0\xi_0$ cylinder for the two temperatures of $T/T_c = 0.8$ and 0.9. The minimum of each L line is also a free energy minimum. These minima are equally spaced and two consecutive ones, associated to L and $L+1$ lines, are separated by $\Delta\mu/\mu_0(0) \approx 9.5$ in agreement with our theoretical analysis that predicts $\Delta\mu/\mu_0(0) = I_1/I_2$, according to Eq.(29). This position is temperature independent and Fig. 4 has a dashed straight line to indicate that for the two temperatures the minimum is in the same magnetic moment value.

Fig. 5 shows the vanishing of the current of each L line for the two temperatures of $T/T_c = 0.8$ and 0.9. The zeros are found to be equally spaced, $\Delta\mu/\mu_0(0) \approx 9.5$, also in agreement with our theoretical analysis that predicts $\Delta\mu/\mu_0(0) = 1/I_1$, according to Eq.(30). The dashed vertical straight line is a guide to the eye to show that the current vanishes at the same magnetic moment independently of the temperature.

Fig. 6 shows the free energy of the tall cylinder ($Z_0 = 10.0\xi_0$) for the temperature of $T/T_c = 0.8$. Distinctly from the short cylinder case, here the minimum of a L line is not a free energy minimum, unless approximately for the first few lines, $L = 0$ to 4. The L lines undergo a transition in shape from the small to the large L limits. To understand this transition we selected the $L = 3$ and 12 lines, also shown in the inset, as they are representative of each side of the transition. While the $L = 3$ line has a single minimum, $L = 12$ has double well shape with two minima at $\mu/\mu_0(0) \approx 130$ and 270, the first one being the lowest one in free energy. Nevertheless the second well is more important than the first one because it sets the true free energy minimum at $\mu/\mu_0(0) \approx 300$, thus away from the L line secondary local minimum. The first one has other competing states with lower energy, the lowest one being the $L = 7$ state, which is drawn as a thick line to help the visualization. The $L = 7$ state is a critical one as it sets the onset of the double well structure. This double well structure is not a feature present in all lines, the first ones simply do not have it. In conclusion the free energy clearly shows two types, single and

double well shaped, that dominate the small and large magnetic moment regimes, respectively. This behavior is also seen in the temperature $T/T_c = 0.9$, as shown in Fig.7. There $L = 5$ is the critical line, and we have also plotted as thick lines, the $L = 3$ and $L = 8$, to show the single to double well transition.

Fig. 8 shows that the $Z_0 = 10.0\xi_0$ cylinder displays novel features as compared to the standard LP problem. The current of the transition L line that separates the single (low L) to the double well (high L) behavior displays unusual behavior. Both limits are characterized by distinct slopes but apart from this both single and double well regions are similar. as shown for the , but not in the transition ($L = 7$) line. This is seen for both temperatures, $T/T_c = 0.8$ and 0.9. The transition lines occur for $L = 7$ and 5, respectively and displays a very unusual current pattern near its zero.

The zeros of the current and the free energy minima coincide for the standard LP, but the inhomogeneous external field sets them apart, as shown here. For this reason we plot the free energy for a given temperature ($T = 0.8T_c$) together with straight vertical lines associated to the zeros of the current. Fig. 9 shows for the $Z_0 = 2.0\xi_0$ cylinder that these straight vertical lines fall very close to the free energy minima in agreement with our theoretical predictions derived in the ring limit. We have selected a few magnetic moment values (red dashed vertical lines) in this diagram for further analysis, given by $\mu/\mu_0 = 9.62$, 66.64, 114.04 and 190.29, whose free energy minima correspond to the $L = 1$, 7 12 and 20 lines. Interestingly we find that these vertical lines intercept the matching points between the $L-1$ and $L+1$ free energy lines up to numerical precision. The distance between consecutive vertical lines is in agreement with the theoretical prediction for $\Delta\mu_c/\mu_0(0) \approx 9.5$. We observe that this property seems to be general, namely, also valid for the $Z_0 = 10.0\xi_0$ cylinder, as shown in Fig. 10. However for the tall cylinder the situation is quite different as the vertical lines clearly form two sets, a low and a high magnetic moment set with a gap between them, located at the $L = 7$ line. The two sets feature distinct separation between consecutive vertical lines with very distinct behavior regarding the free energy minima. The vertical lines of Fig. 10 split into two sets according to their separation. For low values of magnetic moment(until $L = 5$) the distance between two consecutive lines is $\Delta\mu/\mu_0(0) \approx 14.7$. Then, there is a transition region($L = 6, 7, 8$), and for $L > 9$ the curves of the free energy are dominated by the second well. In this region, the distance between the lines is given by $\Delta\mu/\mu_0(0) \approx 30.1$. Comparison betwee tall and short cylinders show that their low magnetic moment has similar behavior, but not for the high magnetic moment regime because of the double well shape of the L lines for the tall cylinder. The zeros of the current are far from the free energy minima and yet they coincide with the crossing of the $L-1$ and $L+1$ free energy lines. In this case we have also selected a few magnetic moment values (red dashed lines) for further analysis: $\mu/\mu_0 = 12.75$, 85.64, 129.02 and 264.97, They are labeled 1, 6, 7 and 11 because they fall within the regimes where these L lines provide the free energy minima.

In the ring limit (very short cylinder) it is easy to verify that the crossing point between any $L-1$ and $L+1$ free energy curves happens at the magnetic moment value of the vanishing of the L state current. In the ring limit the amplitude f is constant and the free energies $\mathcal{F}_{L-1}$ and $\mathcal{F}_{L+1}$ for states $L-1$ and $L+1$, respectively, are given by,

$$\mathcal{F}_{L-1} = -\frac{1}{\beta}[\alpha_0(\frac{\xi_0}{R})^2 g_{L-1} + \alpha(T)]^2, \quad \text{and} \tag{47}$$

$$\mathcal{F}_{L+1} = -\frac{1}{\beta}[\alpha_0(\frac{\xi_0}{R})^2, g_{L+1} + \alpha(T)]^2 \tag{48}$$

according to Eq.(18). Next take that $\mathcal{F}_{L-1} = \mathcal{F}_{L+1}$ to obtain that $g_{L-1}(\mu^*) = g_{L+1}(\mu^*)$, which gives that,

$$\int_{-z0}^{z0} \frac{dz}{Z_0}\Big\{\Big[L - 1 - \frac{\Phi(\mu^*, z)}{\Phi_0}\Big]^2 - \\ -\Big[L + 1 - \frac{\Phi(\mu^*, z)}{\Phi_0}\Big]^2\Big\} = 0, \tag{49}$$

that once simplified becomes,

$$\int_{-z0}^{z0} \frac{dz}{Z_0}\Big[L - \frac{\Phi(\mu^*, z)}{\Phi_0}\Big] = 0 \tag{50}$$

Inserting the definition of the magnetic flux $\Phi(\mu^*, z)$ (Eq.(7)), and expressing the result as a function of integral I_1, previously defined, we obtain that,

$$\frac{\mu^*}{\mu_0} = L\frac{1}{I_1}. \tag{51}$$

This shows that for constant amplitude f it holds that $\mu^* = \mu_c$, according to Eq.(30). We also stress that our present numerical evidence shows that this property also holds for the tall cylinder where the amplitude f is no longer constant.

To gain further insight into the structure of the superconducting state along the cylinder height, we plot in reduced units the current density $J(z)$, the superconducting density $|\psi(z)|^2$, and the potential $V(z)$ as a function of z. Notice that the current loop, which is the source of the inhomogeneous magnetic field, is located in the positive z axis $0.5\xi_0$ above the maximum height. Fig. 11 shows these plots for the $Z_0 = 2.0\xi_0$ cylinder at the selected magnetic moment values called (1), (7), (12) and (20). All the possible crossing L states with the vertical lines, as shown in Fig. 9, are in the $J(z)$, $|\psi(z)|^2$ and $V(z)$ plots. To understand the information given by these plots we start the discussion of the $J(z)$ plots. Because these magnetic moment values are very near to the zeros of the current we take this property to claim that the sought free energy minimum must be such that its $J(z)$ integrated along the z-axis will add to a zero current. Fig. 11(1a) shows that only the $L = 1$ curve qualifies

for a free energy minimum since it is the only one to cross the z-axis thus yielding positive current for $z < 0$ and negative for $z > 0$. According to this criterion all others L lines can be dismissed as they can not be zero current states since they do not cross the z-axis. This reasoning also provides the key to select the free energy minimum in Figs. 11(2a), (3a) and (4a). The present criterion uniquely selects the $L = 7$, 12 and 20 states among the other ones drawn in these figures, respectively, as the only possible free energy minimum because only them fit as zero current states. For the short cylinder the superconducting density $|\psi(z)|^2$, and the potential $V(z)$ also provide features able to uniquely define the sought L lines. For the free energy minimum states the density is nearly constant according to Figs. 11(1b), (2b), (3b) and (4b). Similarly the potential approaches zero for these states as seen in Figs. 11(1c), (2c), (3c) and (4c).

Fig.12 shows these plots for the $Z_0 = 10.0\xi_0$ cylinder at the selected magnetic moment values called (1), (6), (7) and (11). Fig. 12(1a) shows that in the low magnetic moment regime the L state associated to the free energy minimum can be judiciously selected by the zero current condition and this is the $L = 1$ state. The same does not hold for the intermediate magnetic moment values (6) and (7) where many lines qualify at least at the naked eye level precision, which means that many lines cross the z-axis near the center of the cylinder having positive current for $z < 0$ and negative for $z > 0$. For the high magnetic moment limit the situation is similar although the current vanishes near the upper edge of the cylinder, $z \approx 5$, because of the proximity to the strong external current loop. The dramatic changes that the superconducting state undergoes by increasing the magnetic moment are witnessed in the superconducting density $|\psi(z)|^2$, and the potential $V(z)$. Figs. 12(1b), (2b), (3b) and (4b) show that density is mostly concentrated at the top edge of the cylinder for $\mu/\mu_0 = 12.75$ which falls in the low magnetic moment regime. For the intermediate values of $\mu/\mu_0 = 85.64$ and 129.02 we find L states concentrated at both edges to finally find that in the high magnetic moment regime, represented by $\mu/\mu_0 = 264.97$, the density is mostly concentrated at the bottom. Indeed Figs. 12(1c), (2c), (3c) and (4c) show that the potential undergoes dramatic changes from the low to the high magnetic moment regime. In the former case ($\mu/\mu_0 = 85.64$) it undergoes mild changes from one edge to the other as it varies from 0 to 1 in reduced units, while for the latter case($\mu/\mu_0 = 264.97$) it varies from 0 to 23, being very intense in the top edge. These plots explain the reasons for the twofold regimes present in the LP oscillation near the persistent current loop.

V. CONCLUSION

We have considered the Little-Parks oscillations on a thin-walled superconducting cylinder with a persistent (magnetic moment) current loop set on its top. This mesoscopic system is shown here to have two regimes of temperature oscillations not found in the original Little-Parks system because instead of a constant applied magnetic field there is an inhomogeneous magnetic field created in space by the persistent current loop. We observe that this inhomogeneity grows in relevance according to the cylinder height, as expected. In order to unveil the new features we have considered a short and a tall cylinder, and report new results in both cases. For the short cylinder we report new analytical expressions for the magnetic moments associated to the free energy minima, to the zeros of the current, and to the maximum attainable temperature (Eqs.(29), (30) and (31)). For instance, we find that the current in the thin-walled cylinder vanishes at a magnetic moment greater than that of the free energy minimum ($\mu_c \geq \mu_f$). For the tall cylinder we find novel features, perhaps best captured by Fig. 8. This figure shows two distinct current regimes for the tall cylinder, set at low and high L, respectively, associated to distinct slopes with a clear transition L line that separates them. The existence of these two regimes, and the transition that separates them, are within the realm of observable experimental measurements.

VI. ACKNOWLEDGEMENTS

This work is supported by the brazilian agencies CNPq and Facepe.

* mmd@if.ufrj.br

[1] V. V. Moshchalkov, L. Gielen, M. Dhall, C. Van Haesendonck, Y. Bruynseraede, Nature **361**, 617 (1993).

[2] W. A. Little and R. D. Parks, Phys. Rev. Lett. **9**, 9 (1962); R. D. Parks and W. A. Little, Phys. Rev. **133**, A97 (1964).

[3] V. V. Moshchalkov, L. Gielen, C. Strunk, R. Jonckheere, X. Qiu, C. Van Haesendonck, Y. Bruynseraede, Nature **373** 319 (1995).

[4] Mathieu Morelle, Dusan S. Golubovic, and Victor V. Moshchalkov, Physical Review B **70** 144528 (2004).

[5] P.L. Gammel, P.A. Polakos, C.E. Rice, L.R. Harriott, and D.J. Bishop, Phys. Rev. B **41**, 2593 (1990).

[6] Xiaxian Zhang and John C. Price, Phys. Rev. B **55**, 3128 (1997).

[7] O. Bourgeois, S. E. Skipetrov, F. Ong, and J. Chaussy, Phys. Rev. Lett. **94**, 057007 (2005).

[8] Franco Carillo, Gianpaolo Papari, Daniela Stornaiuolo, Detlef Born, Domenico Montemurro, Pasqualantonio Pingue, Fabio Beltram, and Francesco Tafuri, Phys. Rev. B **81**, 054505 (2010)

[9] Hendrik Bluhm, Nicholas C. Koshnick, Martin E. Huber, and Kathryn A. Moler, Phys. Rev. Lett. **97**, 237002 (2006).
[10] Yu. S. Erin, S. V. Kuplevakhski, and A. N. Omelyanchuk, Low Temp. Phys. **34**, 891 (2008).
[11] A. Yu. Aladyshkin, D. A. Ryzhov, A. V. Samokhvalov, D. A. Savinov, A. S. Melnikov, and V. V. Moshchalkov Phys. Rev. B **75**, 184519 (2007).
[12] Jorge Berger and Jacob Rubinstein, Phys. Rev. Lett. **75**, 320 (1995).
[13] Robert Benoist, Wilhelm Zwerger, Z. Phys. B **103**, 377 (1997).
[14] V. Bruyndoncx, L. Van Look, M. Verschuere, and V. V. Moshchalkov, Phys. Rev. B **60**, 10468 (1999).
[15] G.Q. Zha, Eur. Phys. J. B **84**, 459 (2011).
[16] Georg Schwiete, and Yuval Oreg, Phys. Rev. B **82**, 214514 (2010).
[17] L. P. Leévy, G. Dolan, J. Dunsmuir, and H. Bouchiat, Phys. Rev. Lett. **64**, 2074 (1990).
[18] *Foundations of Applied Superconductivity*, Terry P. Orlando and Kevin A. Delin, Addison-Wesley, Reading, MA (1991).
[19] Sebastien Michotte, Damien Lucot and Dominique Mailly, Phys. Rev. B **81**, 100503R (2010).
[20] *Multipole Analysis of Circular Cylindrical Magnetic Systems*, Jerry P. Selvaggi, Ph.D. thesis 2005, Rensselaer Polytechnic Institute, NY. USA.
[21] Felix von Oppen and Eberhard K. Riedel, Phys. Rev. B **46**, 3203 (1992).
[22] G. J. Conduit and Y. Meir, Phys. Rev. B **84**, 064513 (2011).